Chemical Engineering Journal 494 (2024) 152943

Contents lists available at ScienceDirect

Chemical Engineering Journal

journal homepage: www.elsevier.com/locate/cej

Beyond bubbles: Unraveling the interfacial pH effects on bubble size distribution

Jeyse da Silva [a], Eryka Nobrega [a], Felipe Staciaki [a], Fernanda R. Almeida [a], Gabriel Wosiak [a], Alexis Gutierrez [b], Odemir Bruno [b], Mauro C. Lopes [c], Ernesto Pereira [a,*]

[a] Department of Chemistry, Federal University of São Carlos, Universidade Federal de São Carlos, São Carlos, 13565-905, SP, Brazil
[b] Institute of Mathematics and Computer Sciences, University of São Paulo, São Carlos, SP, Brazil
[c] Chemistry Department, State University of Central-West Paraná, 85040-080, Guarapuava, PR, Brazil

ARTICLE INFO

Keywords:
Interfacial pH changes
Bubble dynamics
Electrolysis
Computational image processing
CFD simulation

ABSTRACT

Interfacial pH changes and bubble dynamics play pivotal roles in water electrolysis, significantly impacting cell overvoltage and energy consumption. The quantification of these changes has proven challenging, given the traditional focus on bulk solution pH fluctuations. In contrast to previous studies on individual bubble growth, this research adopts a distinctive approach, analyzing over than 8,000 bubbles in each experiment through advanced image processing computational procedures for edge detection. This methodology provides extensive data for comprehensive statistical analysis. Furthermore, the study delves into the generation of H_2 and O_2 bubbles during water electrolysis in both acidic and alkaline media, employing a platinum strip electrode. Crucial experimental variables, such as electrolyte pH, gas type, and current density, are systematically explored for their influence on bubble size and distribution using a 2^3 factorial design. In addition to this work, finite element simulations were conducted to model interfacial pH under the same experimental conditions. These simulations substantiate our experimental findings, confirming the occurrence of interfacial pH transitions in some instances. This transition, in turn, influences the bubble size distribution and consequently impacts cell voltage. These experimental and simulated datasets and potential curves allow for comparing interfacial pH changes with bubble size and the cell voltage relationship. With broad implications for various applications, such as energy production and material development, where interfacial pH changes and bubble formation are essential, this novel approach allows the optimization of boundary conditions for more effective electrochemical processes.

1. Introduction

The formation of bubbles on the surface of electrodes is a wide-ranging occurrence accompanying many electrochemical processes, especially those involving water as part of the electrolyte [1–4]. This phenomenon has garnered significant interest due to its impact on the electrode surface, catalytic activity, and overall process efficiency [5–7].

The cell overpotential controls the electrochemical process's efficiency, which encompasses activation overpotential, concentration overpotential, and ohmic overpotential [8–10]. Among these, the activation overpotential is notably affected by the formation of gas bubbles. These bubbles cover the electrode surface, leading to inefficient catalytic activity and reducing solution conductivity, further hampering the overall process efficiency [11–17].

Another phenomenon inherent in an aqueous medium's electrochemical process is the electrode–electrolyte interface's pH variation. Electrochemical reactions that consume or produce H^+ and/or OH^- ions create a concentration gradient between the electrode surface and the bulk of the electrolyte [18,19]. The interfacial pH variation changes the boundary conditions around the working electrode (WE), making species available in a different form for the reaction to occur compared to the initial boundary conditions [20–22]. This variation occurs fast just after the beginning of the application of an external potential to the WE. On the other hand, measuring interfacial pH is challenging once conventional techniques cannot measure it. Accurate local pH variations may be detected using methods like Scanning Electrochemical Microscopy (SECM), Scanning Ion-selective Electrode Technique (SIET), and Rotating Ring-Disc Electrode (RRDE); however, these techniques have limitations in temporal or spatial resolution, as well as sensitivity, which restricts their implementation for the *in situ* determination of interfacial pH change in some electrochemical systems

* Corresponding author.
E-mail address: ernesto@ufscar.br (E. Pereira).

https://doi.org/10.1016/j.cej.2024.152943
Received 2 February 2024; Received in revised form 24 May 2024; Accepted 7 June 2024
Available online 10 June 2024

[19,23–26]. In contrast, numerical simulations are a powerful tool for evaluating interfacial pH change when experimental measurements are challenging to accomplish [20,25,27]. Furthermore, the simulation may support experimental results and give extra information that cannot be gained experimentally.

To avoid this undesired efficiency loss, a comprehensive understanding of the behavior of bubble formation and size distribution and the interfacial pH changes in electrochemical processes is required. By associating this phenomenon with energy efficiency, strategies can be identified to manipulate boundary conditions effectively and control gas bubble formation during the process [28–34]. This study presents a comprehensive investigation into the electrochemical production of H_2 and O_2 bubbles during water electrolysis, examining both acidic and alkaline media. While previous research had explored the development of individual bubbles [35–38]. The study employs computational methods for image processing and edge detection to examine approximately 8000 bubbles generated during each experiment. Furthermore, a finite element simulation was used to evaluate the interfacial pH variation under the applied experimental conditions, and the simulation data were correlated with the experimental values of the cell voltage. This work aims to provide valuable insights into enhancing the understanding of electrolysis by comprehensively investigating the dynamics of the correlation between interfacial pH change and bubble size distribution and its effects on the cell overpotential.

2. Methods

2.1. Data acquisition

The experimental setup consists of an electrochemical cell with a rectangular shape made of glass containing two auxiliary electrodes made of polycrystalline platinum grid (1 × 1 cm) positioned to make the current distribution on the working electrode homogeneous. The working electrode is a platinum strip (0.02 × 1 cm) embedded in a glass placed so that the bubbles come out perpendicularly, avoiding the overlap of the objects (bubbles) and keeping the focal distance to the acquisition image system constant. The experimental setup and image processing techniques (depicted in the Supplementary Information) are shown in Fig. 1. For image acquisition, an action camera with fixed focus GoPro Hero 10 model was used to record at 5.3K (5312 × 2988) resolution at 60 frames per second, fps. We set the relative position between the camera and the electrode to optimize the data accuracy. The cell was placed over an XYZ positioner for fine-tuning the focus. A macro lens 55 mm, close-up +10 and a circular polarizer (CLP) filter were used to reduce the focal length and the impact of reflections, respectively. Additionally, we utilized a portable photographic studio NAGANO with dimensions of 60 × 60 × 60 cm, featuring two integrated LED bars for illumination. The top section of the studio houses two built-in light bars, ensuring consistent and adjustable lighting conditions.

Two different solutions were used as electrolyte: KOH 0.1 mol L^{-1} (pH 13) for alkaline medium and $HClO_4$ 0.1 mol L^{-1} (pH 1) for acidic medium. The stoichiometric coefficients of the reactions were used to normalize the current densities in the chronopotentiometric experiments, which produced O_2 and H_2 respectively while maintaining an equal gas flow for both gases.

2.1.1. Image processing techniques

In this work, we use the Edge Detection Method to process the video frames to count the bubbles formed from the electrode to the surface. It is impossible to analyze the frame directly since many kinds of noise are present in the image, such as the scene's illumination, the recipient's color, and the transparent color of the bubbles. Removing all the noise using the following algorithm was necessary to get an accurate result.

Table 1
2^3 factorial design of experiments.

Experiment	Gas	pH	j (mA cm^{-2})
1	O_2	1	50
2	H_2	1	50
3	O_2	13	50
4	H_2	13	50
5	O_2	1	100
6	H_2	1	100
7	O_2	13	100
8	H_2	13	100

2.1.2. Algorithm

The proposed image processing algorithm for addressing bubbles encompasses six sequential steps (Grayscale, Normalization, Edge Detection, Mathematical Morphology, Labeling, and Threshold). Each process segment is visually depicted in Fig. 1 and is fully described in the Supporting Information. This methodological framework encompasses a comprehensive approach to handling different bubble sizes, ultimately contributing to enhanced accuracy and reliability in bubble analysis.

2.2. Chemometric study

A 2^3 full factorial design was carried out to determine the effect of pH, applied current density (j), and gas formed (O_2 and H_2) in the responses, bubble size distribution, and cell potential. The combinations between these independent variables resulted in eight experiments, and all experiments were carried out in duplicate. The experimental conditions are described in the Table 1.

2.2.1. Choose the tiny/big bubble size components

The datasets obtained appear to be a mixture of multiple normal distributions due to overlapping or underlying components. Peaks in the data might represent different sources or components, and the deconvolution of peaks is needed to estimate the bubble size mean values and the standard deviation of the individual normal distributions that compose the observed data. The normalmixEM function from mix tools package [39] version 2.0.0 for the R statistical software [40] version 4.3.2 was used to estimate the parameters of the mixture of normal distributions from observed data, separate the observed data into its constituent parts, and help to identify and characterize individual peaks in the presence of overlapping. The primary objective of the procedure is to determine the parameters associated with the normal distributions, including their amplitudes, standard deviations and means. The algorithm is fully described in the Supporting Information.

2.3. Finite element simulation

We have developed a multiphysics model to evaluate interfacial pH changes during water electrolysis. A simplified one-dimensional geometry was considered to capture the interfacial pH changes efficiently. The model considers a binary electrolyte constrained between two impermeable electrodes, and only the reaction of interest was simulated (cathodic or anodic). The model implementation was based on our previous works, and his full description is presented in the Supplementary Information [20,25].

3. Results and discussion

3.1. Analysis of bubble size distribution

In this study, we employed chemometric methods to extensively evaluate the size distribution of gas bubbles formed during the water electrolysis. This contributes to a deeper understanding of relationships between variables, facilitating the identification of interactions and

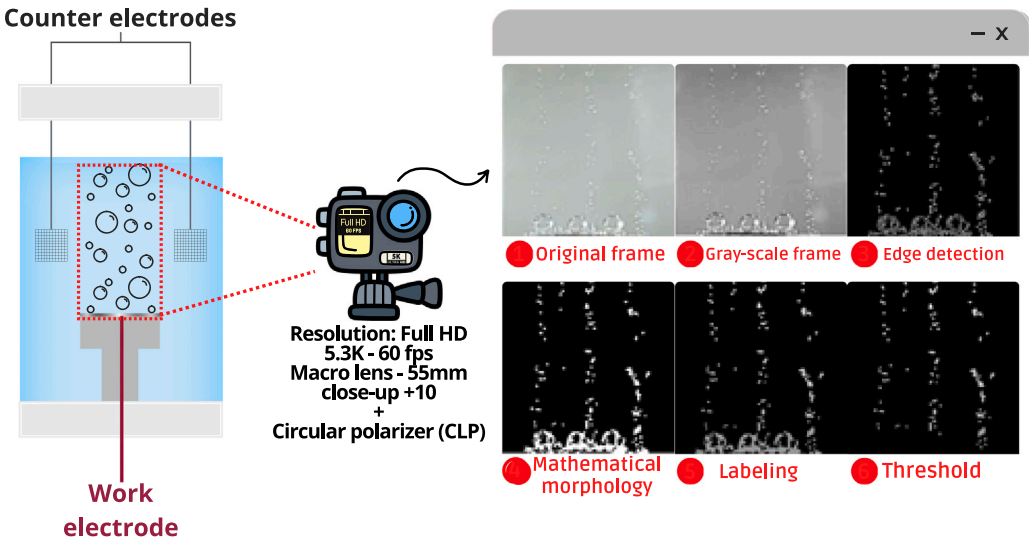

Fig. 1. Image acquisition and processing techniques applied to a single frame. (1): Original frame, (2): Gray-scale frame, (3): Edge detection, (4): Mathematical morphology, (5): Labeling, (6): Threshold.

trends that may go unnoticed in univariate approaches. Minimizing experimental errors and maximizing result reliability are other significant advantages. Thus, employing experimental design saves resources and reduces the time needed to achieve meaningful results. Fig. 2 shows the size distribution of bubbles in experiments 1–8 and the deconvolution component lines, assuming a bimodal distribution and photographs of the electrode's surface.

By iteratively estimating parameters for two normal distributions, including mean values and standard deviations that best align with the data, the algorithm deconvolutes the bimodal distribution. This iterative process enables a thorough exploration of the deconvolution outcomes and facilitates a comprehensive understanding and optimization of the underlying mixture components in the data. Consequently, this approach provides valuable insights into the distinctive characteristics of the underlying components. Such a method is particularly advantageous in scenarios where data originates from two separate sources or processes, allowing for their effective separation and analysis. In the present case, a statistical analysis of the data categorizes it into two groups: tiny bubbles ($d < 150$ μm, characterized by the red deconvolution lines in the histograms) and big bubbles ($d > 150$ μm characterized by the green deconvolution lines).

Fig. 3 was used to assess the significance of ranked variables and to illustrate the influence of these variables and their cross-effects in the response. Effects with a value exceeding the threshold (red lines) are considered statistically significant at $p = 0.05$. This chart illustrates how each variable influenced the percentage of small and large bubbles and indicates the effect's magnitude, direction, and importance.

Notably, the Pareto chart revealed that all the individual variables and their interactions were statistically significant regarding bubble size distribution. Besides, the normalized effect values prominently showcased the magnitude of these influences. Among the variables studied, pH emerged as the most influential, wielding a substantial normalized effect of –7.41. The negative estimated pH effect revealed that the response – the percentage of small over big bubbles – decreased with decreasing pH at the studied variable's values. This finding underscores the paramount role of solution acidity or alkalinity in dictating the resulting bubble sizes. In alignment with the literature's established observations, which indicate that hydrogen bubbles typically exhibit smaller sizes than oxygen bubbles, our study discerns a positive correlation between the gas variable and the bubble size ratio [41–43]. More specifically, our findings reveal a prevalence of tiny bubbles compared to big bubbles. This observation contributes valuable insights to understanding gas-dependent dynamics in bubble formation.

The applied current has shown a significant effect on the system; however, it increases response when it is increased. Surprisingly, the applied current, typically regarded as a straightforward determinant of reaction rate, displayed a comparatively lesser influence on bubble size distribution. This deviation underscores the complexity of electrolytic processes, where multiple factors interweave to shape the outcome. The positive estimated gas type effect revealed that the response increased with the gas type level, indicating that the proportion of tiny bubbles over large ones increases for the formation of O_2. This finding confirms the trend observed in previous studies [44]. While individual analysis of gas and pH variables present their major significance, the gas:pH interaction proves less significant than the third-order gas:pH:j interaction. This discrepancy arises from the negative impact of the pH interaction, contrasting with the positive effects of the gas and j variables. Notably, the j variable enhances the magnitude of this cross-effect due to its significance, contributing to the overall observed effects.

We fitted a first-order equation to make predictions based on the experimental data regarding the percentage of small bubbles over large ones, y. This equation can be formulated and coded as follows:

$$\mathbf{y} = 71.43 + 6.39\mathbf{gas} - 8.59\mathbf{pH} + 3.95\mathbf{J} - 4.50\mathbf{gas}:\mathbf{pH} - 5.98\mathbf{gas}:\mathbf{J} - 4.32\mathbf{pH}:\mathbf{J} + 6.36\mathbf{gas}:\mathbf{pH}:\mathbf{J} \quad (1)$$

In Eq. (1), coefficients with positive values indicate that these terms favor the response, precisely the percentage of tiny bubbles over big bubbles. However, terms with negative coefficients indicate an unfavorable relationship with the response. An analysis of variance (ANOVA) was conducted to justify the significance and adequacy of the regression model. The summary output confirmed the statistical significance of the model at $p = 0.05$. The coefficient of determination (R^2 of 0.958), close to unity, and smaller standard deviation values suggest that the model satisfactorily explains the data variability. The F-value of 26.17 further indicates the model's adequacy and significance. These results imply that the model can account for 96% of the variability in the response, with only 4% attributable to noise.

Traditionally, the literature has reported predictable trends in bubble size distribution. Hydrogen bubbles tend to be smaller than oxygen bubbles due to differences in solubility and diffusion rates [44,45]. Hydrogen gas in a solvent would migrate towards hydrogen bubbles owing to its lower solubility. Additionally, with hydrogen's mass density being approximately 1/16th that of oxygen gas, hydrogen bubbles are more readily detached from the cathode due to their smaller diameter compared to oxygen bubbles, buoyed by the former's lesser mass [46,47].

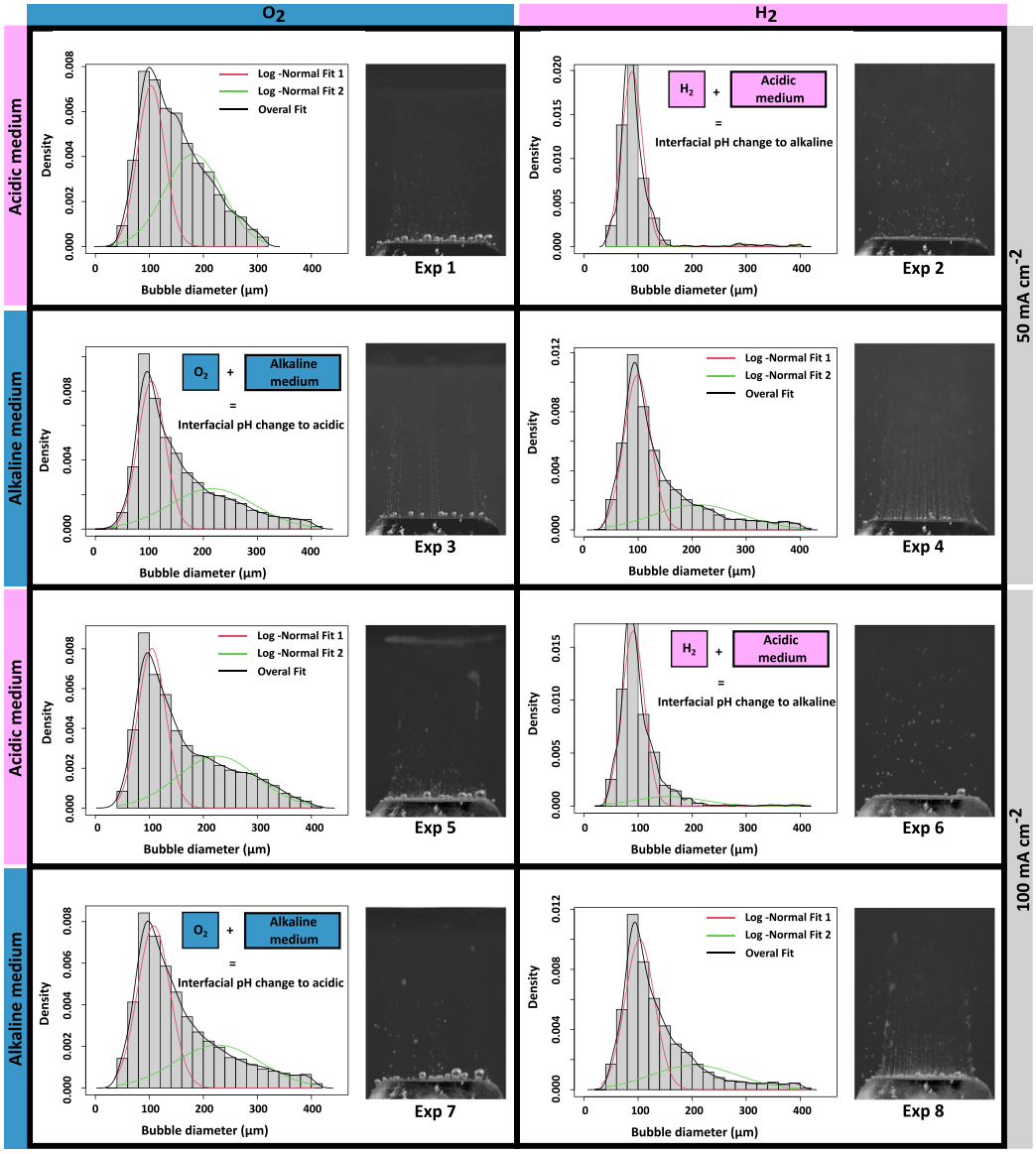

Fig. 2. Bubble size distribution and photographs of the electrode's surface for experiments 1–8.

This is verified in Fig. 2 by comparing each pair of experiments 1–2, 3–4, 5–6, and 7–8.

Alkaline conditions generally yield smaller bubbles than acidic environments. This is due to the influence of hydroxide ions (OH^-) on the surface tension at the electrode–electrolyte interface [48,49]. In acidic environments, H^+ ions enhance the cohesive forces between water molecules, leading to a lower surface tension [50,51]. Conversely, in alkaline environments, the presence of OH^- ions reduces these cohesive forces, resulting in higher surface tension [52–54]. It is important to clarify the relationship between bubble size and surface tension. A higher surface tension in alkaline solutions contributes to smaller bubble sizes, not because of a weakened adhesion to the electrode, but due to the complex interactions at the triple-phase boundary of gas-solid, gas-liquid, and solid–liquid phases [6,55–57]. During bubble growth, the gas-solid interaction at the nucleation point tends to hold the bubble on the electrode. However, surface tension acts in the opposite direction, pulling the bubble away from this interaction [58–61]. Furthermore, studies have shown that the bubble-electrode bonding energy decreases with increasing pH, facilitating earlier detachment of bubbles in more alkaline environments [4]. This is supported by research indicating that as the pH of the solution increases, the diameter of gas bubbles formed on platinum electrodes decreases [62].

This is verified for oxygen bubbles by comparing experiments 1–3 and 5–7. However, hydrogen bubbles show an inverse tendency. While one might expect hydrogen bubbles to exhibit a similar trend to oxygen bubbles in alkaline environments, our observations reveal an inverse tendency. This unexpected behavior can be attributed to the nuanced interplay between the electrochemical reactions occurring at the electrode surface and the variation in interfacial pH. In an alkaline medium, the electrode generating hydrogen experiences a transition from an alkaline to an acidic environment at the electrode surface due to the consumption of hydroxide ions during the oxygen evolution reaction. This transition alters the surface tension dynamics, decreasing surface tension at the electrode–electrolyte interface. As a result, hydrogen bubbles tend to linger longer on the electrode surface, promoting coalescence and the formation of larger bubbles. Likewise, higher current densities are known to generate smaller bubbles due to the enhanced gas evolution rates at the electrode surface [63]. This is verified for oxygen bubbles by comparing experiments 1–5 and 3–7. However, hydrogen bubbles seem to be unaffected by current density. Our experimental findings validate these established trends for experiments 1, 4, 5, and 8, thereby reaffirming the robustness of prior knowledge.

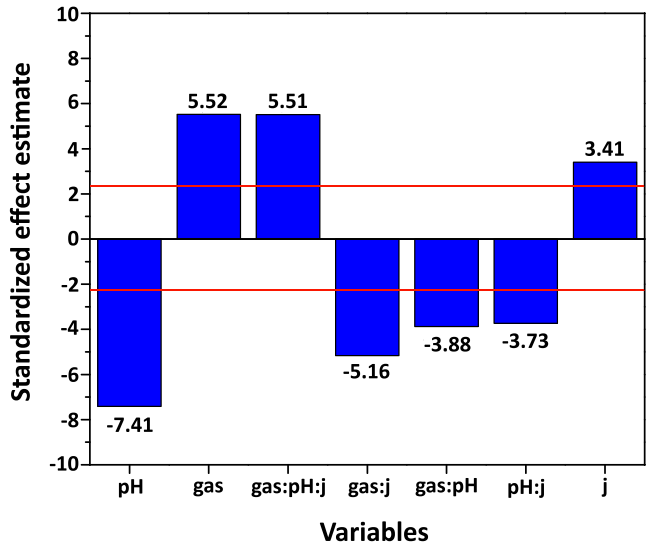

Fig. 3. Pareto plot for the percentage of tiny bubbles/big bubbles.

However, only the tiny bubbles' component line is observed for experiments 2 and 6, in which a bimodal distribution was expected. This outcome is unexpected, given the lower surface tension compared to experiments conducted in an alkaline medium. The same happened to experiments 3 and 7, which were supposed to have an unimodal distribution characterized by tiny bubbles but showed a bimodal distribution, with tiny and big bubbles formed during the experiments. These experiments, conducted in an alkaline medium, would conventionally be anticipated to yield a lower distribution of large bubbles. The intriguing deviations in the bubble size distribution observed in experiments 2, 3, 6, and 7 challenge conventional assumptions and may be closely linked to variations in the interfacial pH. These deviations are particularly surprising given the anticipated influence of heightened surface tension in acidic and alkaline conditions. It is plausible that variations in pH at the electrode–electrolyte interface significantly impact the surface tension and bubble nucleation processes, ultimately leading to the observed distributions. Specifically, the increased concentration of hydronium ions decreases surface tension in acidic conditions, this reduction in surface tension allows gas bubbles to grow larger before detaching from the electrode surface. Conversely, hydroxide ions increase the surface tension in alkaline environments, as a result, gas bubbles formed in alkaline solutions detach more easily from the electrode surface due to the weakened adhesion caused by the higher surface tension.

The data and discussion presented here underscore the importance of considering bubble size distribution in water electrolysis processes. The observed influences of applied current, electrolyte pH, and gas type on bubble characteristics highlight the potential for tailoring bubble formation to enhance reaction efficiency, process stability, and safety. Adopting chemometric methods and image analysis techniques opens new avenues for future research, leading to more informed decisions in the pursuit of sustainable electrochemical processes.

3.2. Relation between bubble size distribution and interfacial pH change

Based on the unexpected trends in the bubble size distribution, we conducted a detailed analysis of the experimental chronopotentiometry curves for each experiment to elucidate the relationship between the proposed changes in the interfacial pH and the potential behavior.

Fig. 4 shows the potential curves for the eight experiments of the experimental design. It can be observed that the potential curves for experiments 2, 3, 6, and 7 exhibit interesting behaviors with the formation of two plateaus in comparison to experiments 1, 4, 5, and 8. These peculiarities may be attributed to the interfacial pH changes expected under the experimental conditions of the four experiments mentioned above, as documented in the literature [18,20,64–66]. This transition, driven by intricate electrochemical processes at the electrode–electrolyte interface, introduces dynamic changes to the composition of surface-active species. Consequently, the behavior of the electrolytic system is perturbed, resulting in unexpected bubble size distribution.

During water electrolysis, one of the half-reactions constantly undergoes a significant pH variation at the electrode–electrolyte interface. Fig. 5 represents how the electrode and solution interact during water electrolysis. It also shows how changes in pH at the electrode interface are closely linked to specific electrochemical reactions, H_2 evolution in an acidic medium, and O_2 evolution in an alkaline medium.

As shown in Fig. 5A, the cathodic reaction takes place in an acidic environment, which creates H_2 by using up H^+ ions on the electrode surface. After the consumption of H^+ species, the water itself begins to be reduced, leading to the formation of OH^- ions. Consequently, this consumption of species results in a change in the interfacial pH from acidic to alkaline, in contrast to the bulk pH. Moving to Fig. 5B, the anodic reaction takes place to produce O_2 in an alkaline medium. During this stage of the reaction, there is a consumption of OH^- ions, yielding O_2 and H_2O. In the same way as with an acidic medium, H_2O is oxidized to make O_2 and H^+ ions after OH^- species are used up. Consequently, the pH at the interface transitions from alkaline to acidic during the O_2 formation process. In all cases, the interfacial pH change generates a concentration overpotential. As the reaction conditions are no longer the same as the initial ones, the cell potential increases its value to maintain the electrode current constant. The results presented here emphasize the central role of pH variations in shaping both bubble size distribution and cell potential during water electrolysis.

To obtain a relationship between the cell potential values and the variables studied, the overpotential values were obtained from the extrapolation of the asymptotic potential and subtracted from the Nernst potential values.

$$\eta = E_{cell} - E_{Nernst} \tag{2}$$

where

$$E_{Nernst} = 1.229V - 0.0591 * pH_{bulk} \tag{3}$$

To achieve this, we utilized data derived from each experiment's extrapolation of chronopotentiometry curves to the asymptotic potential (the complete description of the method is described in the Supplementary Information). This approach offers a comprehensive assessment of the electrochemical behavior under different operating conditions. The extrapolation technique employed in this study is a well-established method in electrochemistry for estimating overpotentials, as supported by previous works [67–72]. It provides a robust method to characterize the performance of electrochemical systems. By extending the chronoamperometric data to the asymptotic potential, we effectively captured the limiting behavior of the electrochemical processes under investigation.

As shown in Table 2, the experimental conditions that exhibit higher overpotentials are those where interfacial pH transition is expected. The experiments with the interfacial pH transition alkaline→acidic (experiments 3 and 7) have a higher overpotential than those for the same gas where these phenomena do not occur (experiments 1 and 5). This overpotential can be related to concentration overpotential and Ohmic and activation overpotential since the pH changes directly affect the bubble size distribution and, consequently, the electrode surface coverage. However, when the interfacial pH changes acidic→alkaline (experiments 2 and 6), the overpotential is smaller than the experiments for the same gas that does not present these phenomena (4 and 8). One possibility to explain this behavior is the change in the bubble size distribution occasioned by the different surface tension led

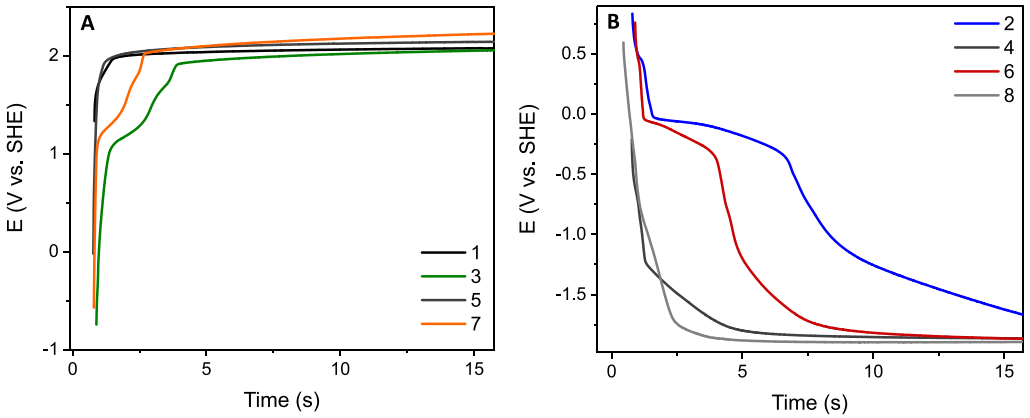

Fig. 4. Potential curves for experiments 1–8; (A) for O_2 and (B) for H_2.

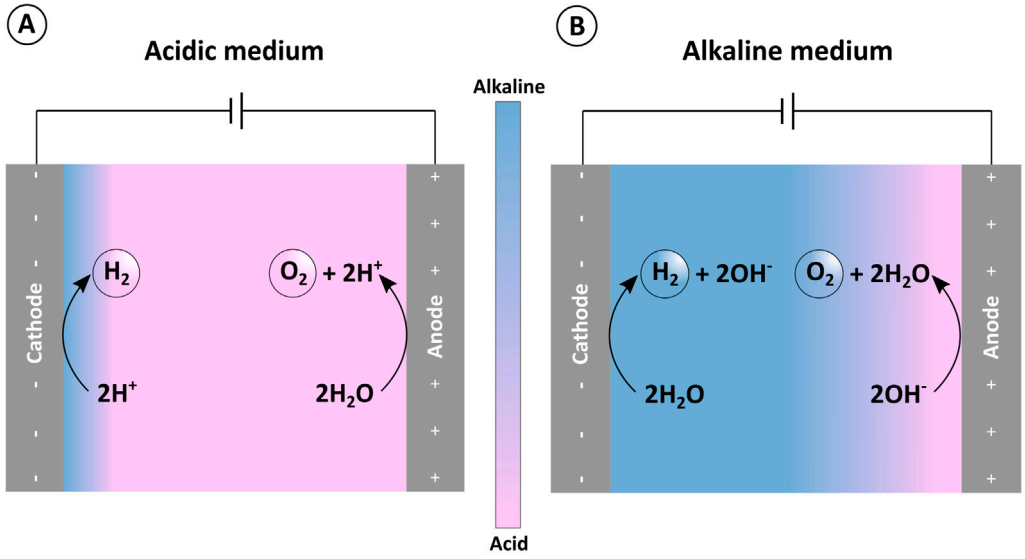

Fig. 5. Schematic representation of the reactions that lead to the interfacial pH transition in (A) acidic and (B) alkaline medium.

Table 2
Overpotential values and interfacial pH for experiments 1–8.

Exp	Gas	pH	j (mA cm^{-2})	η (V)	Interfacial pH
1	O_2	1	50	0.95 ± 0.01	Acidic
2	H_2	1	50	0.77 ± 0.02	Acidic → Alkaline
3	O_2	13	50	1.85 ± 0.1	Alkaline → Acidic
4	H_2	13	50	1.32 ± 0.02	Alkaline
5	O_2	1	100	1.03 ± 0.01	Acidic
6	H_2	1	100	0.80 ± 0.02	Acidic → Alkaline
7	O_2	13	100	2.12 ± 0.05	Alkaline → Acidic
8	H_2	13	100	1.57 ± 0.003	Alkaline

by the accumulation of OH^- species in the interface electrode solution. Then, the formation of smaller bubbles occurs, decreasing the resulting overpotential.

A notable finding of our study is the strong correlation between bubble size distribution and cell potential. Analyzing the obtained data, we observed distinct trends in the cell potential corresponding to different experimental conditions. Experiments 2, 3, 6, and 7 exhibited unique profiles in contrast to the expected behavior for constant-current water electrolysis. This deviation from the anticipated behavior can be attributed to the interaction between pH variations and electrochemical reactions at the electrode surface.

Despite the size distribution showing a higher quantity of large bubbles in experiments 3 and 7, the large bubbles formed remained on the electrode surface, taking longer to detach compared to experiments 4 and 8. This could be why a higher overpotential is observed, even though both experiments have the same pH and current density. This difference can be explained by the interfacial pH change, which occurs in experiments 3 and 7 but not in experiments 4 and 8. Consequently, the solution-electrode interface becomes acidic in experiments 3 and 7, increasing the surface tension and making the bubble's detachment process from the electrode more difficult, promoting their coalescence.

The correlation between cell potential and bubble size distribution substantiates the interdependence of these two parameters. It reinforces the notion that the properties of the gas bubbles formed are intrinsically linked to the electrochemical processes occurring at the electrode–electrolyte interface. The data, therefore, indicate that monitoring bubble size distribution could indirectly assess cell potential variations and vice versa.

The results of the overpotential were also treated as a response to the experimental design used in this investigation, and its Pareto's chart is presented in Fig. 6. Notably, the Pareto chart revealed that all the individual variables gas type, pH, and applied current density were statistically significant when overpotential was used as a response at $p = 0.05$. In addition, just the gas:pH and pH:j interactions were statistically significant concerning the overpotential.

Based on the experimental data related to the overpotential (η), we developed a first-order equation for predictive purposes. This equation

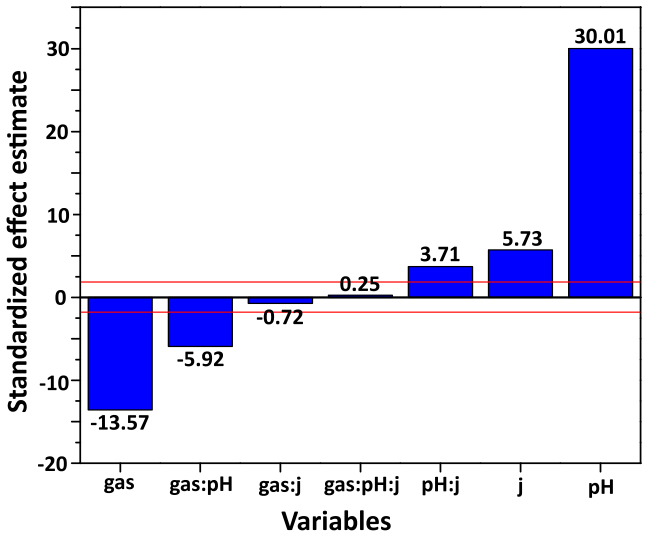

Fig. 6. Pareto plot for overpotential with significance lines.

can be formulated and coded as follows:

$$\eta = 1.30 - 0.19\mathbf{gas} + 0.41\mathbf{pH} + 0.08\mathbf{J} - 0.08\mathbf{gas} : \mathbf{pH} + 0.05\mathbf{pH} : \mathbf{j} \quad (4)$$

In Eq. (4), coefficients with a negative impact indicate terms that contribute to decreasing the response in terms of η. Conversely, coefficients with a positive influence denote terms that contribute to an augmentation in the response concerning overpotential. To assess the significance and suitability of the regression model, we carried out an ANOVA, and the summarized results confirmed the statistical importance of the model at a significance threshold of $p = 0.05$. The determination coefficient (R^2 of 0.993), coupled with reduced standard deviation values, implies that the model effectively accommodates the variability in the data. The F-value of 166.7 further reinforces the model's appropriateness and significance. These outcomes propose that the model can elucidate nearly 99% of the variability in the response, with only 1% ascribed to noise.

The gas variable exhibits a more pronounced negative impact, indicating that the overpotential is lower when the evolved gas is H_2. This can be attributed to the smaller size of H_2 bubbles than O_2. Additionally, the lower density of H_2 and the disparity in solubility between these gases affect bubble formation dynamics, leading to significant electrode coverage and a notable reduction in overpotential. On the other hand, the pH and current variables demonstrate a positive effect, indicating that higher pH or current results in increased overpotential. This suggests a direct relationship between pH or current intensity and overpotential magnitude. Additionally, the interaction between gas type and pH has been identified as a significant determinant in overpotential modification. While first-order variables are traditionally more influential, our observations support that the specific interaction between O_2 gas in an alkaline environment and H_2 in an acidic environment induces substantial changes in overpotential. This phenomenon is attributed to interfacial pH variation, resulting in the complete transformation of the environment at the surface-electrode interface.

In this sense, we employed a Computational Fluid Dynamics (CFD) approach utilizing COMSOL Multiphysics to gain deeper insights into the electrochemical processes. This enabled us to computationally simulate the interfacial pH at the working electrode during the initial seconds of experiments 1 and 2.

Fig. 7 shows the experimental and simulated data for two separate experiments, Experiment 1 (Fig. 7A) and Experiment 2 (Fig. 7B). It shows how the cell potential changed over time (experimental) and how the interfacial pH changed (simulated).

Fig. 7A depicts the cell potential and interfacial pH in the O_2 evolution reaction. Noteworthy is the observation that both the interfacial pH and cell potential exhibit non-significant variations throughout the experiment. Fig. 7B presents the potential curve alongside the simulated interfacial pH for the H_2 evolution reaction over time. The shaded region, marked by a color gradient, reveals a striking change in potential and a pH transition. Initially acidic, the pH undergoes an abrupt transition to alkaline within a short time frame, coinciding with the observed shift in potential.

We propose that the observed abrupt change in the cell potential is intrinsically linked to the pH transition and a change in the morphology of the bubbles, as these two processes unfold simultaneously. Analyzing the cell voltage and the simulated interfacial pH, we can assume that the abrupt variations in voltage are directly related to the interfacial pH transition. However, a discrepancy between the interfacial pH and cell voltage in the transition region can be observed. We propose that this difference can be explained by the convective movement generated by the bubble detachment during electrolysis. As verified in previous work of our group [73], convection is promoted by the gas bubble's detachment from the electrode surface. This movement leads to a higher bubble detachment at the electrode edges and in the mixing of species present at the electrode/solution interface. The computational model used focused only on electrochemical reactions, neglecting the dynamics of bubbles in the solution due to the difficulty of model convergence and the computational effort required to simulate the interfacial pH transition region. Therefore, the gas bubble dynamics could attenuate the interfacial pH transition by the convective movement promoted by bubble detachment, since the mixture of species can lead to neutralization of OH^- with H^+ species [73–75]

Therefore, the unexpected behavior in the bubble size distribution in experiments 2, 3, 6, and 7 can be justified by the intense variation in interfacial pH that occurs under these conditions. These observations show that interfacial pH is pivotal in dictating the bubble size distribution. This, in turn, has a cascading effect on the overall cell potential.

Our methodology provided an in-depth understanding of the interplay between various parameters and bubble size distribution. Such insights can be valuable in optimizing the design and operation of many electrochemical systems.

4. Conclusions

This study explored the dynamics between experimental parameters, bubble size distribution, interfacial pH changes, and cell potential in electrochemical water electrolysis. We unraveled intricate relationships underpinning the system's behavior by systematically varying pH, applied current, and gas type.

We have observed through careful statistical analysis that the change in pH dramatically affects the electrochemical reactions at the interface between the electrode and the electrolyte. The observed differences in bubble shape and cell potential from what would be expected show how pH changes and electrochemical kinetics work together in complex ways. Notably, our study revealed a strong correlation between bubble size distribution and cell potential, suggesting that monitoring the former could be a proxy for assessing the latter.

The phenomenon of interfacial pH variation emerged as a central theme in this work. We established its presence as a driving force behind the observed experimental outcomes, reaffirming the phenomenon's significance in electrochemical processes. Moreover, finite element simulations were used to model interfacial pH under the same experimental conditions. This confirmed our experimental results and gave us more information about how pH changes affect bubble shape and cell potential.

These findings have implications beyond fundamental research, as they can inform the design and optimization of electrochemical systems for practical applications such as hydrogen production.

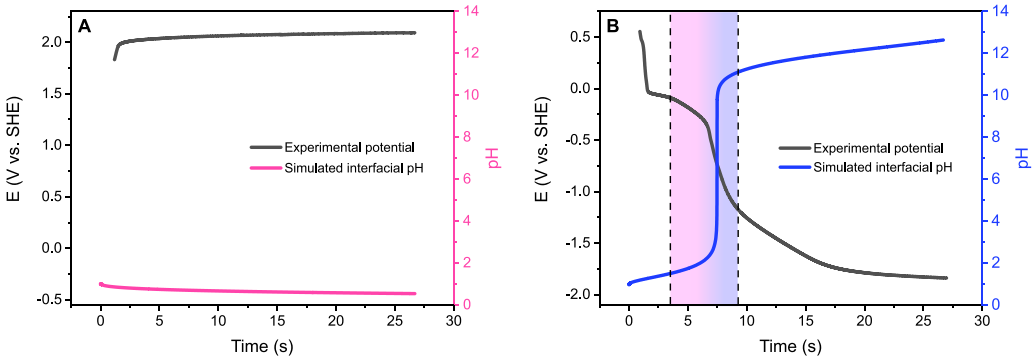

Fig. 7. Experimental chronopotentiometry curves and simulated interfacial pH for experiment 1 (A) - O_2 evolution reaction in acidic medium, and 2 (B) - H_2 evolution reaction in acidic medium.

In conclusion, this study enriches our knowledge of the intricate interplay between pH variations, bubble size distribution, and cell potential in electrochemical water electrolysis. By shedding light on the underlying mechanisms and integrating simulation results, we contribute to a broader understanding of electrochemical systems and open avenues for innovation in sustainable energy technologies.

CRediT authorship contribution statement

Jeyse da Silva: Writing – review & editing, Writing – original draft, Visualization, Validation, Methodology, Investigation, Formal analysis, Data curation, Conceptualization. **Eryka Nobrega:** Writing – review & editing, Writing – original draft, Methodology, Investigation, Formal analysis. **Felipe Staciaki:** Writing – review & editing, Writing – original draft, Methodology, Investigation, Formal analysis, Conceptualization. **Fernanda R. Almeida:** Writing – review & editing, Investigation, Formal analysis. **Gabriel Wosiak:** Writing – review & editing, Methodology, Data curation, Conceptualization. **Alexis Gutierrez:** Software, Data curation. **Odemir Bruno:** Writing – review & editing, Supervision, Software, Formal analysis, Data curation. **Mauro C. Lopes:** Writing – review & editing, Supervision, Software, Investigation, Formal analysis, Conceptualization. **Ernesto Pereira:** Writing – review & editing, Supervision, Resources, Project administration, Investigation, Funding acquisition, Conceptualization.

Declaration of competing interest

The authors declare that they have no known competing financial interests or personal relationships that could have appeared to influence the work reported in this paper.

Data availability

Data will be made available on request.

Acknowledgments

Financial support is provided by FAPESP (2013/07296-2, 2014/50249-8, 2015/12851-0, 2017/11986-5, 2018/24383-0, 2019/27029-5, 2021/11630-1, 2022/05254-0), Shell, CNPq (407878/2022-0), and CAPES (Code 001).

Appendix A. Supplementary data

Supplementary material related to this article can be found online at https://doi.org/10.1016/j.cej.2024.152943.

References

[1] H. Qiu, K. Obata, Z. Yuan, T. Nishimoto, Y. Lee, K. Nagato, I. Kinefuchi, J. Shiomi, K. Takanabe, Quantitative description of bubble formation in response to electrolyte engineering, Langmuir 39 (14) (2023) 4993–5001, http://dx.doi.org/10.1021/acs.langmuir.2c03488.

[2] K.M. Cho, P.R. Deshmukh, W.G. Shin, Hydrodynamic behavior of bubbles at gas-evolving electrode in ultrasonic field during water electrolysis, Ultrason. Sonochem. 80 (2021) http://dx.doi.org/10.1016/j.ultsonch.2021.105796.

[3] Y. Ma, Z. Guo, Q. Chen, X. Zhang, Dynamic equilibrium model for surface nanobubbles in electrochemistry, Langmuir : ACS J. Surf. Colloids (2021).

[4] Q. Zhu, W. Tarpeh, Developing in situ electrochemical techniques to understand mechanisms of bubble formation at aqueous electrochemical interfaces, in: ECS Meeting Abstracts, 2022.

[5] J.R. Lake, A.M. Soto, K.K. Varanasi, Impact of bubbles on electrochemically Active Surface Area of microtextured gas-evolving electrodes, Langmuir 38 (10) (2022) 3276–3283, http://dx.doi.org/10.1021/acs.langmuir.2c00035.

[6] A. Angulo, P. van der Linde, H. Gardeniers, M. Modestino, D. Fernández Rivas, Influence of bubbles on the energy conversion efficiency of electrochemical reactors, Joule 4 (3) (2020) 555–579, http://dx.doi.org/10.1016/j.joule.2020.01.005.

[7] C. Lee, B. Zhao, J. Lee, K. Fahy, K. Krause, A. Bazylak, Bubble formation in the electrolyte triggers voltage instability in CO2 electrolyzers, iScience (2020).

[8] Z. Qiu, D. Martín-Yerga, P.A. Lindén, G. Henriksson, A. Cornell, Green hydrogen production via electrochemical conversion of components from alkaline carbohydrate degradation, Int. J. Hydrog. Energy 47 (6) (2022) 3644–3654, http://dx.doi.org/10.1016/j.ijhydene.2021.11.046.

[9] S. Wang, A. Lu, C.-J. Zhong, Hydrogen production from water electrolysis: role of catalysts, Nano Converg. 8 (1) (2021) 1–23, http://dx.doi.org/10.1186/s40580-021-00254-x.

[10] J.A. Wrubel, C. Milleville, E. Klein, J. Zack, A.M. Park, G. Bender, Estimating the energy requirement for hydrogen production in proton exchange membrane electrolysis cells using rapid operando hydrogen crossover analysis, Int. J. Hydrog. Energy 47 (66) (2022) 28244–28253, http://dx.doi.org/10.1016/j.ijhydene.2022.06.155.

[11] Y. Liu, X. Lu, Y. Peng, Q. Chen, Electrochemical visualization of gas bubbles on superaerophobic electrodes using scanning electrochemical cell microscopy, Anal. Chem. 93 (36) (2021) 12337–12345, http://dx.doi.org/10.1021/acs.analchem.1c02099.

[12] Ö. Akay, J. Poon, C. Robertson, F.F. Abdi, B.R. Cuenya, M. Giersig, K. Brinkert, Releasing the bubbles: Nanotopographical electrocatalyst design for efficient photoelectrochemical hydrogen production in microgravity environment, Adv. Sci. 9 (8) (2022) 2105380, http://dx.doi.org/10.1002/advs.202105380.

[13] N. Dubouis, A. Grimaud, The hydrogen evolution reaction: from material to interfacial descriptors, Chem. Sci. 10 (40) (2019) 9165–9181, http://dx.doi.org/10.1039/C9SC03831K.

[14] J. Dukovic, C.W. Tobias, The influence of attached bubbles on potential drop and current distribution at gas-evolving electrodes, J. Electrochem. Soc. 134 (2) (1987) 331, http://dx.doi.org/10.1149/1.2100456.

[15] S. Park, L. Liu, Ç. Demirkır, O. van der Heijden, D. Lohse, D. Krug, M.T.M. Koper, Solutal Marangoni effect determines bubble dynamics during electrocatalytic hydrogen evolution, Nature Chem. (2023) 1–9, http://dx.doi.org/10.1038/s41557-023-01294-y.

[16] G.F. Swiegers, R.N.L. Terrett, G. Tsekouras, T. Tsuzuki, R.J. Pace, R. Stranger, The prospects of developing a highly energy-efficient water electrolyser by eliminating or mitigating bubble effects, Sustain. Energy Fuels 5 (5) (2021) 1280–1310, http://dx.doi.org/10.1039/D0SE01886D.

[17] M.M. Bakker, D.A. Vermaas, Gas bubble removal in alkaline water electrolysis with utilization of pressure swings, Electrochim. Acta 319 (2019) 148–157, http://dx.doi.org/10.1016/j.electacta.2019.06.049.

[18] M.C.O. Monteiro, X. Liu, B.J.L. Hagedoorn, D.D. Snabilié, M.T.M. Koper, Interfacial pH measurements using a rotating ring-disc electrode with a voltammetric pH sensor, ChemElectroChem 9 (1) (2022) e202101223, http://dx.doi.org/10.1002/celc.202101223.

[19] W. Chen, M.-K. Zhang, B.-Y. Liu, J. Cai, Y.-X. Chen, Challenges and recent progress in unraveling the intrinsic pH effect in electrocatalysis, Curr. Opin. Electrochem. 34 (2022) 101003, http://dx.doi.org/10.1016/j.coelec.2022.101003.

[20] G. Wosiak, M.C. Silva, J. da Silva, E.B. Carneiro-Neto, M.C. Lopes, E. Pereira, Evaluation of interfacial pH change during water splitting at pulsed regime using finite element method, Int. J. Hydrog. Energy 46 (34) (2021) 17644–17652, http://dx.doi.org/10.1016/j.ijhydene.2021.02.195.

[21] X. Liu, M.C.O. Monteiro, M.T.M. Koper, Interfacial pH measurements during CO2 reduction on gold using a rotating ring-disk electrode, Phys. Chem. Chem. Phys. 25 (4) (2023) 2897–2906, http://dx.doi.org/10.1039/D2CP05515E.

[22] G.A. Kamat, J.A. Zamora Zeledón, G.T.K.K. Gunasooriya, S.M. Dull, J.T. Perryman, J.K. Nørskov, M.B. Stevens, T.F. Jaramillo, Acid anion electrolyte effects on platinum for oxygen and hydrogen electrocatalysis, Commun. Chem. 5 (20) (2022) 1–10, http://dx.doi.org/10.1038/s42004-022-00635-1.

[23] M.C.O. Monteiro, M.T.M. Koper, Measuring local pH in electrochemistry, Curr. Opin. Electrochem. 25 (2021) 100649, http://dx.doi.org/10.1016/j.coelec.2020.100649.

[24] K.-C. Deng, Z.-X. Lu, J.-J. Sun, J.-Y. Ye, F. Dong, H.-S. Su, K. Yang, M.M. Sartin, S. Yan, J. Cheng, Z.-Y. Zhou, B. Ren, Accelerated interfacial proton transfer for promoting electrocatalytic activity, Chem. Sci. 13 (36) (2022) 10884–10890, http://dx.doi.org/10.1039/D2SC01750D.

[25] E.B. Carneiro-Neto, M.C. Lopes, E.C. Pereira, Simulation of interfacial pH changes during hydrogen evolution reaction, J. Electroanal. Chem. 765 (2016) 92–99, http://dx.doi.org/10.1016/j.jelechem.2015.09.029.

[26] A.M. Zimer, M. Medina da Silva, E.G. Machado, H. Varela, L.H. Mascaro, E.C. Pereira, Development of a versatile rotating ring-disc electrode for in situ pH measurements, Anal. Chim. Acta 897 (2015) 17–23, http://dx.doi.org/10.1016/j.aca.2015.09.047.

[27] J. Wu, W. Zheng, Y. Chen, Factors affecting the cathode/electrolyte interfacial pH change during water reduction: A simulation study, Int. J. Hydrog. Energy 47 (43) (2022) 18597–18605, http://dx.doi.org/10.1016/j.ijhydene.2022.04.035.

[28] K.w.W.M. (Kees), Avoiding bubble troubles: Investigating the relationship between bubbles and electrochemistry, Phys.org (2020).

[29] T. Kadyk, D. Bruce, M. Eikerling, How to enhance gas removal from porous electrodes? Sci. Rep. 6 (38780) (2016) 1–14, http://dx.doi.org/10.1038/srep38780.

[30] C. Deslouis, I. Frateur, G. Maurin, B. Tribollet, Interfacial pH measurement during the reduction of dissolved oxygen in a submerged impinging jet cell, J. Appl. Electrochem. 27 (4) (1997) 482–492, http://dx.doi.org/10.1023/A:1018430224622.

[31] J.P. O'Reilly, C.P. Butts, I.A. I'Anso, A.M. Shaw, Interfacial pH at an isolated silica-water surface, J. Am. Chem. Soc. 127 (6) (2005) 1632–1633, http://dx.doi.org/10.1021/ja0443326.

[32] E. Carneiro-Neto, M. Lopes, E. Pereira, Simulation of interfacial pH changes during hydrogen evolution reaction, J. Electroanal. Chem. 765 (2015) http://dx.doi.org/10.1016/j.jelechem.2015.09.029.

[33] T. Coward, J.G.M. Lee, G.S. Caldwell, The effect of bubble size on the efficiency and economics of harvesting microalgae by foam flotation, J. Appl. Phycol. 27 (2) (2015) 733–742, http://dx.doi.org/10.1007/s10811-014-0384-5.

[34] Q. Sun, H. Gu, X. Yu, W. Yin, Bubble formation characteristic of submerged single-hole orifice in aerosol suspension, Front. Energy Res. 7 (2019) 475691, http://dx.doi.org/10.3389/fenrg.2019.00092.

[35] X. Deng, Y. Shan, X. Meng, Z. Yu, X. Lu, Y. Ma, J. Zhao, D. Qiu, X. Zhang, Y. Liu, Q. Chen, Direct measuring of single–heterogeneous bubble nucleation mediated by surface topology, Proc. Natl. Acad. Sci. USA 119 (29) (2022) e2205827119, http://dx.doi.org/10.1073/pnas.2205827119.

[36] Y. Qiu, H. Ren, M.A. Edwards, R. Gao, K. Barman, H.S. White, Electrochemical generation of individual nanobubbles comprising H2, D2, and HD, Langmuir 36 (22) (2020) 6073–6078, http://dx.doi.org/10.1021/acs.langmuir.0c00232.

[37] S.R. German, M.A. Edwards, Q. Chen, Y. Liu, L. Luo, H.S. White, Electrochemistry of single nanobubbles. Estimating the critical size of bubble-forming nuclei for gas-evolving electrode reactions, Faraday Discuss. 193 (2016) 223–240, http://dx.doi.org/10.1039/C6FD00099A.

[38] Q. Chen, L. Luo, H. Faraji, S.W. Feldberg, H.S. White, Electrochemical measurements of single H2 nanobubble nucleation and stability at Pt nanoelectrodes, J. Phys. Chem. Lett. 5 (20) (2014) 3539–3544, http://dx.doi.org/10.1021/jz501898r.

[39] T. Benaglia, D. Chauveau, D.R. Hunter, D.S. Young, Mixtools: An R package for analyzing mixture models, J. Stat. Softw. 32 (2010) 1–29, http://dx.doi.org/10.18637/jss.v032.i06.

[40] R Core Team, R: A Language and Environment for Statistical Computing, R Foundation for Statistical Computing, Vienna, Austria, 2023.

[41] L.J. Janssen, C.W. Sillen, E. Barendrecht, S.J. van Stralen, Bubble behaviour during oxygen and hydrogen evolution at transparent electrodes in KOH solution, Electrochim. Acta 29 (5) (1984) 633–642, http://dx.doi.org/10.1016/0013-4686(84)87122-4.

[42] J.J. Bikerman, Surface Chemistry: Theory and Applications, Elsevier Science, Oxford, England, UK, 2013.

[43] Y. Li, G. Yang, S. Yu, Z. Kang, J. Mo, B. Han, D.A. Talley, F.-Y. Zhang, In-situ investigation and modeling of electrochemical reactions with simultaneous oxygen and hydrogen microbubble evolutions in water electrolysis, Int. J. Hydrog. Energy 44 (52) (2019) 28283–28293, http://dx.doi.org/10.1016/j.ijhydene.2019.09.044.

[44] K. Matsuura, Y. Yamanishi, C. Guan, S. Yanase, Control of hydrogen bubble plume during electrolysis of water, J. Phys. Commun. 3 (3) (2019) 035012, http://dx.doi.org/10.1088/2399-6528/ab0c30.

[45] C. Jiménez, B. Talavera, C. Sáez, P. Cañizares, M.A. Rodrigo, Study of the production of hydrogen bubbles at low current densities for electroflotation processes, J. Chem. Technol. Biotechnol. 85 (10) (2010) 1368–1373, http://dx.doi.org/10.1002/jctb.2442.

[46] E.L. Cussler, Diffusion: Mass Transfer in Fluid Systems, Cambridge University Press, 2009.

[47] N.I. Kolev, N.I. Kolev, Multiphase Flow Dynamics: Fundamentals, vol. 1, Springer, 2005.

[48] D. Zhang, K. Zeng, Evaluating the behavior of electrolytic gas bubbles and their effect on the cell voltage in alkaline water electrolysis, Ind. Eng. Chem. Res. 51 (42) (2012) 13825–13832, http://dx.doi.org/10.1021/ie301029e.

[49] R.R. Hacha, A.G. Merma, H.J.B. Couto, M.L. Torem, Measurement and analysis of H2 and O2 bubbles diameter produced by electroflotation processes in a modified partridge-smith cell, Powder Technol. 342 (2019) 308–320, http://dx.doi.org/10.1016/j.powtec.2018.09.062.

[50] R. Kronberg, K. Laasonen, Dynamics and surface propensity of H+ and OH– within rigid interfacial water: Implications for electrocatalysis, J. Phys. Chem. Lett. 12 (41) (2021) 10128–10134, http://dx.doi.org/10.1021/acs.jpclett.1c02493.

[51] R.E. Khoma, A.A. Ennan, R.M. Dlubovskii, Y.V. Ishkov, T.S. Bienkovska, E.M. Rakhlitskaya, Equilibrium processes in AlkNHCH2SO3H–NH2CH2CH2OH–H2O solutions, Russ. J. Gen. Chem. 91 (4) (2021) 583–592, http://dx.doi.org/10.1134/S1070363221040010.

[52] R. Vácha, D. Horinek, M.L. Berkowitz, P. Jungwirth, Hydronium and hydroxide at the interface between water and hydrophobic media, Phys. Chem. Chem. Phys. 10 (32) (2008) 4975–4980, http://dx.doi.org/10.1039/B806432F.

[53] C. Tian, N. Ji, G.A. Waychunas, Y.R. Shen, Interfacial structures of acidic and basic aqueous solutions, J. Am. Chem. Soc. 130 (39) (2008) 13033–13039, http://dx.doi.org/10.1021/ja8021297.

[54] B. Jagoda-Cwiklik, L. Cwiklik, P. Jungwirth, Behavior of the eigen form of hydronium at the air/water interface, J. Phys. Chem. A 115 (23) (2011) 5881–5886, http://dx.doi.org/10.1021/jp110078s.

[55] E. Virga, E. Spruijt, W.M. de Vos, P.M. Biesheuvel, Wettability of amphoteric surfaces: The effect of pH and ionic strength on surface ionization and wetting, Langmuir 34 (50) (2018) 15174–15180, http://dx.doi.org/10.1021/acs.langmuir.8b02875.

[56] C. Meng, B. Wang, Z. Gao, Z. Liu, Q. Zhang, J. Zhai, Insight into the role of surface wettability in electrocatalytic hydrogen evolution reactions using light-sensitive nanotubular TiO2 supported pt electrodes, Sci. Rep. 7 (41825) (2017) 1–8, http://dx.doi.org/10.1038/srep41825.

[57] G. Duhar, C. Colin, Dynamics of bubble growth and detachment in a viscous shear flow, Phys. Fluids 18 (7) (2006) http://dx.doi.org/10.1063/1.2213638.

[58] R. Massoudi, A.D. King Jr., Effect of pressure on the surface tension of water. Adsorption of low molecular weight gases on water at 25°, J. Phys. Chem. 78 (22) (1974) 2262–2266, http://dx.doi.org/10.1021/j100615a017.

[59] O.R. Enríquez, C. Hummelink, G.W. Bruggert, D. Lohse, A. Prosperetti, D. Van Der Meer, C. Sun, Growing bubbles in a slightly supersaturated liquid solution, Rev. Sci. Instrum. 84 (6) (2013) http://dx.doi.org/10.1063/1.4810852.

[60] Á. Moreno Soto, Bubbles on Surfaces: Diffusive Growth & Electrolysis, Álvaro Moreno Soto, Physics of Fluids Group, University of Twente, The Netherlands, 2019.

[61] S. Lubetkin, The motion of electrolytic gas bubbles near electrodes, Electrochim. Acta 48 (4) (2002) 357–375, http://dx.doi.org/10.1016/S0013-4686(02)00682-5.

[62] N.P. Brandon, G.H. Kelsall, Growth kinetics of bubbles electrogenerated at microelectrodes, J. Appl. Electrochem. 15 (4) (1985) 475–484, http://dx.doi.org/10.1007/BF01059288.

[63] P. Chandran, S. Bakshi, D. Chatterjee, Study on the characteristics of hydrogen bubble formation and its transport during electrolysis of water, Chem. Eng. Sci. 138 (2015) 99–109, http://dx.doi.org/10.1016/j.ces.2015.07.041.

[64] I. Ledezma-Yanez, W.D.Z. Wallace, P. Sebastián-Pascual, V. Climent, J.M. Feliu, M.T.M. Koper, Interfacial water reorganization as a pH-dependent descriptor of the hydrogen evolution rate on platinum electrodes, Nat. Energy 2 (17031) (2017) 1–7, http://dx.doi.org/10.1038/nenergy.2017.31.

[65] P. Li, Y. Jiang, Y. Hu, Y. Men, Y. Liu, W. Cai, S. Chen, Hydrogen bond network connectivity in the electric double layer dominates the kinetic pH effect in hydrogen electrocatalysis on Pt, Nat. Catal. 5 (10) (2022) 900–911, http://dx.doi.org/10.1038/s41929-022-00846-8.

[66] P. Bollella, A. Melman, E. Katz, Electrochemically generated interfacial pH change: Application to signal-triggered molecule release, ChemElectroChem 7 (16) (2020) 3386–3403, http://dx.doi.org/10.1002/celc.202000615.

[67] M.G. Hennessy, I.R. Moyles, Asymptotic reduction and homogenization of a thermo-electrochemical model for a lithium-ion battery, Appl. Math. Model. 80 (2020) 724–754, http://dx.doi.org/10.1016/j.apm.2019.11.018.

[68] A.J. Sous, Asymptotic iteration method applied to new confining potentials, Pramana 93 (2) (2019) 22–25, http://dx.doi.org/10.1007/s12043-019-1782-7.

[69] I.R. Moyles, M.G. Hennessy, T.G. Myers, B.R. Wetton, Asymptotic reduction of a porous electrode model for lithium-ion batteries, SIAM J. Appl. Math. (2019).

[70] G. Richardson, J.R. King, Time-dependent modelling and asymptotic analysis of electrochemical cells, J. Engrg. Math. 59 (3) (2007) 239–275, http://dx.doi.org/10.1007/s10665-006-9114-6.

[71] L.L. Frumin, G.V. Zilberstein, Asymptotic approach in steady-state electrode kinetics for the spherical electrode, J. Electrochem. Soc. 144 (10) (1997) 3458, http://dx.doi.org/10.1149/1.1838032.

[72] R.J. Drachman, Asymptotic effective potentials for electron-hydrogen scattering, J. Phys. B: At. Mol. Phys. 12 (22) (1979) L699, http://dx.doi.org/10.1088/0022-3700/12/22/009.

[73] G. Wosiak, J. da Silva, S.S. Sena, R.N. de Andrade, E. Pereira, CFD simulation and experimental comparison of bubble-induced convection during electrochemical water splitting, Chem. Eng. J. 433 (2022) 133194, http://dx.doi.org/10.1016/j.cej.2021.133194.

[74] K. Obata, F.F. Abdi, Bubble-induced convection stabilizes the local pH during solar water splitting in neutral pH electrolytes, Sustain. Energy Fuels 5 (15) (2021) 3791–3801, http://dx.doi.org/10.1039/D1SE00679G.

[75] L.M. Baumgartner, A. Kahn, M. Hoogland, J. Bleeker, W.F. Jager, D.A. Vermaas, Direct imaging of local pH reveals bubble-induced mixing in a CO2 electrolyzer, ACS Sustain. Chem. Eng. 11 (28) (2023) 10430–10440, http://dx.doi.org/10.1021/acssuschemeng.3c01773.